Invented Forces in Supercell Models

ROBERT DAVIES-JONES[a]

[a] *NOAA/National Severe Storms Laboratory, Norman, Oklahoma*

(Manuscript received 16 March 2021, in final form 22 June 2021)

ABSTRACT: This paper examines methods used in supercell models to maintain a steady, sheared, horizontally uniform environment with a three-force balance in the planetary boundary layer (PBL) and a two-force balance above it. Steady environments are maintained while ignoring the thermal-wind balance that permits large shear above the PBL. The Taylor–Proudman theorem indicates that wind profiles above the PBL must be unidirectional for balanced environments. In principle, supercell models that do not accommodate thermal advection should not support balanced steady environments with veering horizontally uniform winds. Recent methods add a permanent, pervasive, horizontal external force that varies only with height. By adding two more degrees of freedom, this force circumvents the Taylor–Proudman theorem and enables a static, horizontally uniform environment for any wind profile. It succeeds by adding spurious energy in lieu of flow toward low pressure to offset frictional loss of kinetic energy. However, the artificial force has downsides. It decouples the environmental horizontal equation of motion from the hydrostatic equation and the thermodynamics from the dynamics. It cancels environmental friction and the part of the Coriolis force that acts on the environmental wind. Within the storm, its curl can speciously generate significant horizontal vorticity near the ground. Inaccuracies arise in circulations around material circuits because of modifications by the artificial force and resulting miscalculations of parcel trajectories. Doubt is cast on conclusions about tornadogenesis drawn from recent simulations that contain an invented force.

SIGNIFICANCE STATEMENT: Before entering a tornado, air parcels spin predominantly about a horizontal axis because of torques exerted by buoyancy and frictional forces. The relative importance of these torques in tornado formation is undecided. Because in situ data collected in severe storms are sparse, observations are insufficient for identifying origins of spin. Scientists resort instead to diagnosing detailed results provided by computer simulations of storms that develop in tornado-favorable environments. To simplify physical interpretation, the environment is fixed in some simulations by use of a substantial ubiquitous and permanent artificial force. I demonstrate that this strategem leads to suspect conclusions about tornado formation. Issues arise because the invented force loosens flow constraints, alters parcel trajectories, performs spurious work, and generates horizontal spin falsely.

KEYWORDS: Tornadogenesis; Storm environments; Supercells; Vorticity

1. Introduction

In meteorology, the laws governing mass, energy, momentum, angular momentum, and entropy, should be sacrosanct. In supercell simulations, invented forces should be tolerated only to the extent that they do not fundamentally alter the results. The latest supercell simulations with surface drag have such high resolution that they reproduce strong to violent tornadoes. These simulations seek to understand tornadogenesis. Use of a fictitious force that generates spurious horizontal vorticity and energy (Roberts et al. 2016, 2020; hereinafter R16 and R20, respectively) obscures conclusions about the physical causes of tornadogenesis.

Difficulties also arise when laws are applied only to a base state and not to deviations from it. For example, mass excesses and deficits arise in supercell models when the continuity equation is satisfied only in the base state. This nonconservation of mass may affect the maximum wind speeds and pressure deficits of tornadoes that form within simulated supercells.

A supercell model solves the governing equations subject to suitable initial and boundary conditions. From a mathematical perspective, the chosen initial conditions are arbitrary. Ideally the initial conditions should not be too far from an equilibrium state as minor changes in initial conditions can result sometimes in very different outcomes. Physically, they should be reasonably realizable. Otherwise, large ''shocks to the system'' affect the subsequent evolution unrealistically. A model can be initialized with a single environmental sounding as long as the environment is allowed to evolve.

Some modelers, however, desire a specified, unchanging, horizontally uniform environment in which to grow storms. A static environment specified by a single sounding is possible only if the environmental initial state is a steady-state solution of the governing equations. The possibility also exists that a steady solution is unstable. Because of the Taylor–Proudman theorem (Tritton 1988, p. 218), a stipulated static environment is not generally a steady solution. Modelers circumvent this problem by adding a fictitious horizontal force to Newton's second law of motion. They are then solving the wrong equations. The additional two degrees of freedom associated with the unnatural force allow the environment to be fixed. Unfortunately

Davies-Jones's status: Emeritus.

Corresponding author: Robert Davies-Jones, bobdj1066@yahoo.com

DOI: 10.1175/JAS-D-21-0082.1

the required external force, which is a surrogate for the horizontal pressure-gradient force (HPGF) that would exist in a horizontally varying environment, is permanent, pervasive, and a function of height z only. Fixing the environment, thus, changes the dynamics inside the storm.

When the invented force is small relative to, say, the HPGF in a mesocyclone, we might expect that its presence is benign. For instance, Wilhelmson and Chen (1982) allowed the Coriolis force to act only on deviations from the environmental wind. This is equivalent to using an invented force that cancels the Coriolis force in the environment.

However, above the PBL, the invented force has to replace the large-scale HPGF and balance the Coriolis force in order to maintain a static horizontally uniform environment. Use of the external force instead of the HPGF uncouples the horizontal equation of motion from the other equations governing the environment. In the presence of vertical wind shear and Coriolis forces, a real balanced environment must have a horizontal thermodynamic gradient. Strongly sheared supercell environments are baroclinic, not horizontally uniform. In an unrealistic, static, horizontally uniform environment, there is no baroclinity and the Rossby number (ratio of inertial to Coriolis forces) is zero because the horizontal length scale is infinite. Under these conditions, the Taylor–Proudman theorem dictates that the wind shear must vanish above the PBL if the model is run without a storm. If we allow a horizontal density gradient, then we find below that a steady sheared environment with horizontally uniform winds is possible only if the atmosphere above the PBL is equivalent barotropic, which is still uncharacteristic of supercell environments.

The invented force can cause graver problems when there is friction in the environment. When the lower boundary condition is free slip, the stratification is stable enough, and turbulence is not introduced artificially, zero eddy viscosity is a solution of the model sans storm (Markowski and Bryan 2016, hereinafter MB16). But serious difficulties arise in simulations that implement surface drag and hence activate friction near the ground. To prevent diminishing environmental winds, supercell modelers allow surface drag to affect only the wind deviation (e.g., Wilhelmson and Chen 1982; Adlerman and Droegemeier 2002). This amounts to inventing a force $\mathbf{K}(z)$ that cancels the environmental frictional force $\mathbf{F}_0$ and the environmental Coriolis force $\mathbf{C}_0$ (if present), thus, enabling a static horizontally uniform environment. If the modeler does not impose significant random perturbations to excite turbulence and the stratification is sufficiently stable, the parameterization scheme that simulates the effects of turbulence on subgrid scales is active in the environment only in a very shallow surface layer (MB16). Then the shear stress, which is specified at the ground by the semislip boundary condition, vanishes at a low height above the ground. Consequently $\mathbf{F}_0$, which is the vertical derivative of shear stress, is large in a shallow surface layer. Since $\mathbf{K}$ cancels $\mathbf{F}_0$ and $\mathbf{C}_0$, it too is large next to the ground. This is evident in Fig. 8 in Dawson et al. (2019, hereinafter DRX19) where $\mathbf{K}$ exceeds $10^{-2}\,\mathrm{m\,s^{-2}}$ near the ground. Inside the storm, $\mathbf{K}(z)$ is the same as outside of it but is no longer balanced by the frictional and Coriolis forces. This unbalanced artificial force harms the simulation.

Tornadogenesis depends critically on near-surface processes so the presence of a significant artificial unbalanced force $\mathbf{K}(z)$ near the ground is not conducive to its understanding. Because $\mathbf{K}$ balances the frictional and Coriolis forces in the environment, it is affected greatly by the model's parameterization of turbulence. Unfortunately, supercell models do not perform well next to the ground for three reasons. First, because of use of a staggered grid, the horizontal resolved wind is not defined at the ground itself. The lowest level at which it is defined is one-half of a vertical grid spacing above the ground (the "lowest scalar level"). Second, large-eddy simulation (LES) has a known weakness next to the ground where the dynamically important eddies are unresolved (Davidson 2015, p. 402; discussed further in section 3). Third, as demonstrated by MB16, the vertical profile of the frictional force in LES is unrealistic if random perturbations with sufficient amplitude are not introduced into the flow to excite significant turbulence.

As shown herein, an invented force is clearly no panacea because it manufactures false accelerations, false energy, false horizontal vorticity, and false contributions to circulations around inaccurately calculated material circuits. [Circuits that dip below the lowest scalar level are not trusted even without an invented force (Dahl et al. 2012)]. Conclusions about tornadogenesis drawn from recent simulations using a permanent external force therefore seem questionable. These studies conclude that that a tornado may originate from frictional rather than baroclinic vorticity. Obviously part of the vertical vorticity of a rotating updraft ultimately is generated by environmental frictional torques. It stems from vorticity generated by the shear stress at the ground, diffused into the PBL, and ultimately tilted and stretched by the updraft. Friction is also vital in the contraction of a tornado cyclone into a tornado that breaks the thermodynamic speed limit (Fiedler and Rotunno 1986). Thus, frictional interaction of the airflow with the ground is believed to play an important role in tornadogenesis. However, parameterized frictional torques may be generating too much horizontal vorticity in too shallow a surface layer, thus, making tornadogenesis too rapid. As shown by Rotunno et al. (2017), uplifting of excessive near-ground horizontal vorticity results in significant vertical vorticity at very low heights.

2. Unnatural initialization of supercell models

For reasons listed by DRX19 (4035–4036) and R20 (p. 1703), modelers often covet an ideal, static, horizontally uniform environment. Consequently, many supercell models use a single sounding for initialization and set up a steady environmental flow without horizontal gradients by using an artificial force. In contrast, the observed wind profile in the PBL has a flow component toward low pressure, so the atmospheric environment varies horizontally. Without imposition of an external force, a horizontally uniform environment with Coriolis force and vertical wind shear is never in equilibrium because of thermal-wind imbalance above the PBL. The environment evolves by developing secondary circulations that tend to restore geostrophic balance (Holton 1992, section 6.4).

For a simulation initialized with a single sounding, establishing thermal-wind balance with a vertical shear of around

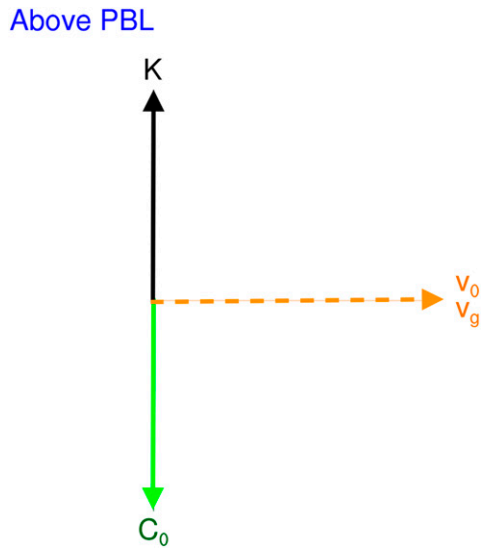

FIG. 1. The force balance in the environment above the PBL. The environmental wind $\mathbf{v}_0$ and the environmental geostrophic wind $\mathbf{v}_g$ are dashed orange vectors. In this case $\mathbf{v}_0$ and $\mathbf{v}_g$ are identical. The Coriolis force $\mathbf{C}_0$ (green solid vector) is directed 90° to the right of $\mathbf{v}_0$. In supercell models with a horizontally uniform environment, $\mathbf{C}_0$ is balanced by a made-up force $\mathbf{K}$ (black solid vector) instead of by a horizontal pressure-gradient force.

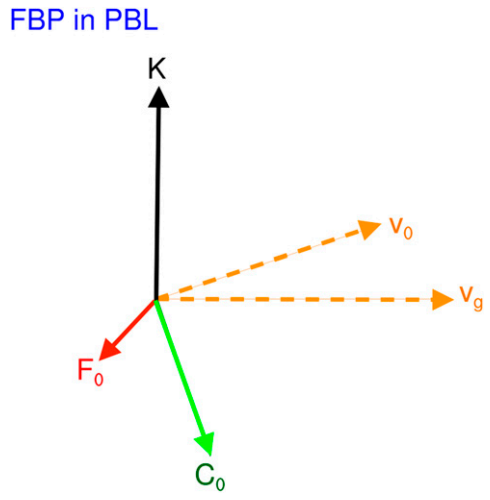

FIG. 2. As in Fig. 1, but for the three-force balance within the PBL for the FBP. In this case the environmental wind $\mathbf{v}_0$ is different from environmental geostrophic wind $\mathbf{v}_g$. The invented force $\mathbf{K}$ is 90° to the left of $\mathbf{v}_g$. The $\mathbf{v}_0$ is determined by $f(\mathbf{v}_0 - \mathbf{v}_g)$ being directed 90° to the right of frictional force $\mathbf{F}_0$ and having the same magnitude as $\mathbf{F}_0$. The $\mathbf{K}$ balances $\mathbf{F}_0$ (red solid vector) and the Coriolis force $\mathbf{C}_0$, which is 90° to the right of $\mathbf{v}_0$. The positive spurious energy $\mathbf{v}_0 \cdot \mathbf{K}$ offsets the frictional loss of kinetic energy $\mathbf{v}_0 \cdot \mathbf{F}_0$.

$10^{-2}\,\mathrm{s}^{-1}$ requires a linear horizontal temperature gradient of around 3 K $(100\,\mathrm{km})^{-1}$. Replacing the environmental HPGF with an invented force is advantageous because it eliminates the need for this temperature gradient. An actual sounding already incorporates the effect of friction in the Ekman layer. However, the parameterized friction and heat fluxes in the model are imperfect matches to atmospheric turbulence. Without an environmental HPGF, the model's surface drag and internal frictional forces would rapidly modify the environmental wind profile over time, especially near the ground, as kinetic energy would dissipate rapidly. Another advantage of an external force is that it performs work to negate this energy loss. We shall see, however, that the invented force also has its downsides.

There are three recent techniques to incorporating surface drag into simulations. The first two methods use a spurious horizontal force to constrain the environment to be static and horizontally uniform. The artificial force added to Newton's second law of motion introduces two extra degrees of freedom, thus, allowing the supplemented model equations to have superfluous solutions. The first approach (R16; Roberts and Xue 2017, hereinafter RX17; Coffer and Parker 2017), called the frictional balancing procedure (FBP) by R20, takes a proximity hodograph representative of the environment and modifies it (Figs. 1 and 2). This procedure is discussed further in section 7.

The second approach (DRX19; Oliveira et al. 2019; R20), which supersedes the first, is called the geotriptic wind balance (GWB) method. It uses a horizontally uniform environment that is hydrostatically balanced and in three-way equilibrium between the Coriolis force, the parameterized turbulent frictional force, and an invented force $\mathbf{K}(z)$ (Figs. 1 and 3). This method is evaluated in section 8.

The third approach utilizes nested models and so does not start from a horizontally uniform state. Since it does not use an invented force, it is beyond the scope of this paper. We should note, however, that the tornadoes in these simulations do not occur early in a storm's lifetime and that diagnostics find that the vorticity origins of many of the tornadoes are frictional

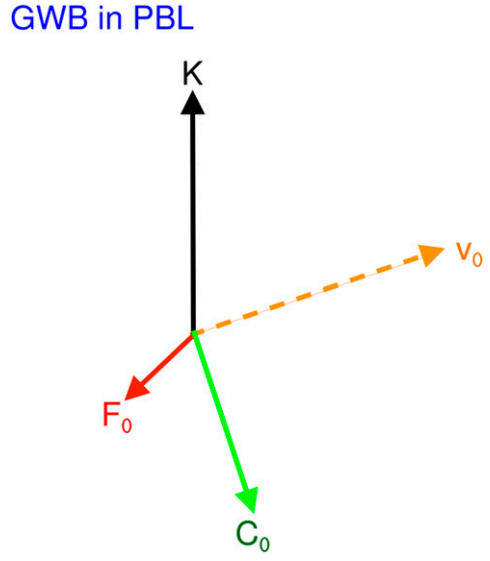

FIG. 3. As in Fig. 2, but for the three-force balance within the PBL for the GWB. Here the invented force $\mathbf{K}$ does not depend on environmental geostrophic wind $\mathbf{v}_g$.

FIG. 4. Example of a warm bubble perturbing a horizontally uniform environment. Laminar condensation rings reveal waves propagating outward from the bubble into the environment where the TKE is small. In this test (Castle Bravo on 1 Mar 1954), mass was not conserved exactly and the environment was not restored.

rather than baroclinic (e.g., Schenkman et al. 2014; Mashiko 2016; Tao and Tamura 2020).

Early storm development is influenced by convective initiation as well as by the specified environment. Convection is often initialized in a supercell model by releasing a warm bubble at low levels. A large bubble is used to overcome any convective inhibition and in environments without a cap to obtain an isolated long-lived supercell instead of narrow towering cumuli that cannot withstand the shear (Davies-Jones 2002). The hope is that, in the long run, storm structure becomes independent of the initial conditions, namely the way that the environment was upset to trigger the storm. The bubble is inserted into the initial conditions as a strong temperature perturbation without any initial adjustment whatsoever to the wind field and the vortex lines. In an extreme case, a wide bubble with a large 6-K amplitude in a very unstable environment with a lifted index of −10.5 K and a lot of streamwise vorticity establishes an intense rotating updraft atypically soon. The environment that is intended to remain horizontally uniform and steady is upset by gravity and sound waves radiating outward from the rising thermal (as exemplified by Fig. 4). As the updraft intensifies at low levels, high winds, abnormally strong low-level convergence, and a tornado intensified by the effort of surface drag, all develop at the surface within 30 min of convective initiation.

3. Short description of supercell models

For later use, we present a simplified but representative set of equations that are adequate for illustrating an idealized dry supercell model. The equations governing motion, mass continuity, and entropy on an f plane in the Northern Hemisphere (where the Coriolis parameter $f > 0$) are

$$\frac{d\mathbf{v}}{dt} = -f\mathbf{k}\times\mathbf{v} - \frac{1}{\rho}\nabla p - g\mathbf{k} + \mathbf{F} + \mathbf{K}(z), \tag{1}$$

$$\frac{d\ln\rho}{dt} + \nabla\cdot\mathbf{v} = 0, \quad \text{and} \tag{2}$$

$$\frac{d\ln\theta}{dt} = \frac{R}{c_p}\frac{1}{p}\frac{\delta Q}{\delta t} + \frac{D}{\theta} \equiv \frac{\dot\theta}{\theta}, \tag{3}$$

respectively, where t is time, $\mathbf{v}$ is the wind vector, $d/dt \equiv \partial/\partial t + \mathbf{v}\cdot\nabla$ is the material derivative, ρ is density, p is pressure, θ is potential temperature, g is the gravitational acceleration, $\mathbf{F}$ is the divergence of the turbulent subgrid-scale momentum flux per unit mass (loosely called the frictional force), and $\mathbf{K}(z)$ is a spurious horizontal force. The rate of potential temperature change per unit mass is $\dot\theta$, $\delta Q/\delta t$ is the rate that heat is added per unit volume, D is the divergence of the turbulent theta-flux vector, R is the gas constant, and c_p is the specific heat at constant pressure. The equation of state is

$$\rho\theta = \frac{p_{00}}{R}\left(\frac{p}{p_{00}}\right)^{1/\gamma}, \tag{4}$$

where $\gamma \equiv c_p/c_v$, c_v is the specific heat at constant volume, and p_{00} is a standard pressure (1000 hPa). The entropy $S = c_p\ln\theta$ up to an additive constant, and the temperature $T = \theta(p/p_{00})^{\kappa}$, where $\kappa = R/c_p$. In terms of eastward, northward, and vertical unit vectors $\mathbf{i}$, $\mathbf{j}$, $\mathbf{k}$, respectively, the position vector is $\mathbf{x} \equiv x\mathbf{i} + y\mathbf{j} + z\mathbf{k} \equiv x_1\mathbf{i} + x_2\mathbf{j} + x_3\mathbf{k}$, and the wind vector is $\mathbf{v} \equiv u\mathbf{i} + v\mathbf{j} + w\mathbf{k} \equiv u_1\mathbf{i} + u_2\mathbf{j} + u_3\mathbf{k}$.

Equations (1)–(4) form a closed set of prognostic equations in the variables $\mathbf{v}$, ρ, p, and θ. The prognostic equation for mass in (2) is often replaced by a combination of (2) and (3), namely,

$$\frac{d\ln(\rho\theta)}{dt} + \nabla\cdot\mathbf{v} = \frac{\dot\theta}{\theta}, \tag{5}$$

where

$$\ln(\rho\theta) = \frac{1}{\gamma}\ln p \tag{6}$$

by (4). From (5) and (6) we obtain the prognostic equation for pressure:

$$\frac{d\ln p^{1/\gamma}}{dt} + \nabla\cdot\mathbf{v} = \frac{\dot{\theta}}{\theta}, \tag{7}$$

or, equivalently,

$$\frac{\partial p^{1/\gamma}}{\partial t} + \nabla\cdot(p^{1/\gamma}\mathbf{v}) = p^{1/\gamma}\frac{\dot{\theta}}{\theta}. \tag{8}$$

Most cloud models avoid solving a diagnostic pressure equation by instead solving a system of fully prognostic partial differential equations for compressible flow such as (1), (3), and (8). The numerical method utilizes a splitting technique wherein low-amplitude dynamically insignificant sound waves are treated separately using a smaller time step than for the nonacoustic flow features (Klemp and Wilhelmson 1978). Models typically define a base state, which is a function of height alone and is simply a motionless hydrostatic atmosphere. Variables are expressed as the sum of basic-state parts denoted by subscript 0 and deviation values denoted by subscript 1. Then (8) usually is approximated as

$$\frac{\partial p_1^{1/\gamma}}{\partial t} + \nabla\cdot(p_0^{1/\gamma}\mathbf{v}) = p_0^{1/\gamma}\frac{\dot{\theta}}{\theta_0}. \tag{9}$$

The first term enables sound-wave propagation, but mass is not conserved accurately because it is not deemed crucial (Klemp and Wilhelmson 1978, p. 1073; Wilhelmson and Wicker 2001, p. 126). The steady version of (9),

$$\nabla\cdot(p_0^{1/\gamma}\mathbf{v}) = p_0^{1/\gamma}\frac{\dot{\theta}}{\theta_0}, \tag{10}$$

is the pseudoincompressible continuity equation (Durran 1989). Thus, the simple mass continuity equation in (2) ends up being replaced by a hybrid continuity-thermodynamic equation in (8) that contains the *parameterized* subgrid-scale term D via (3). Since there are no sound waves to filter in a steady environmental flow and we want accurate mass conservation that does not involve parameterized heat fluxes, we generally retain (2).

We obtain the following equation for parcel energy by taking the dot product of (1) and $\mathbf{v}$:

$$\frac{d}{dt}\left(\frac{\mathbf{v}\cdot\mathbf{v}}{2} + gz\right) = -\frac{1}{\rho}\mathbf{v}\cdot\nabla p + \mathbf{v}\cdot\mathbf{F} + \mathbf{v}\cdot\mathbf{K}(z). \tag{11}$$

The sum of a parcel's kinetic energy and potential energy is equal to the works performed on the parcel by the pressure-gradient force (PGF), $\mathbf{F}$, and $\mathbf{K}$.

The equation for relative vorticity $\boldsymbol{\zeta} \equiv \nabla\times\mathbf{v}$ is

$$\frac{d\boldsymbol{\zeta}}{dt} = (\boldsymbol{\zeta}\cdot\nabla)\mathbf{v} + f\frac{\partial\mathbf{v}}{\partial z} - (\nabla\cdot\mathbf{v})(\boldsymbol{\zeta}+f\mathbf{k})\boldsymbol{\omega} - \nabla\alpha\times\nabla p + \nabla\times\mathbf{F} + \nabla\times\mathbf{K}(z) \tag{12}$$

(Dutton 1976, p. 338), where $\alpha \equiv 1/\rho$ is the specific volume and $-\nabla\alpha\times\nabla p$, the curl of the PGF, is the baroclinity vector $\mathbf{B}$ (Dutton 1976, p. 374). From (12) and (2) the steady-state vorticity equation for an environment with small Rossby number is

$$0 = \mathbf{B} + f\mathbf{v}\cdot\nabla\ln\rho\mathbf{k} + f\frac{\partial\mathbf{v}}{\partial z} + \nabla\times(\mathbf{F}+\mathbf{K}). \tag{13}$$

In a steady state in the free atmosphere with $\mathbf{K}\equiv 0$, 1) solenoidal generation of horizontal vorticity must cancel the horizontal vorticity produced by tilting of Earth's vertical vorticity by the shear flow and 2) solenoidal generation of vertical vorticity must cancel the density-advection term in (13). Conclusion 2 holds even with an invented force $\mathbf{K}(z)$ since its curl has no vertical component.

Tornadogenesis diagnostics frequently utilize a circulation theorem. Integrating (1) around a material circuit $C(t)$ yields the circulation equation:

$$\frac{d}{dt}\oint_{C(t)}\mathbf{v}\cdot d\mathbf{x} = \oint_{C(t)} p\,d\alpha - f\oint_{C(t)}(\mathbf{k}\times\mathbf{v})\cdot d\mathbf{x} + \oint_{C(t)}\mathbf{F}\cdot d\mathbf{x} + \oint_{C(t)}\mathbf{K}(z)\cdot d\mathbf{x}, \tag{14}$$

where the force circulations on the right in order are the baroclinic, Coriolis, frictional, and spurious ones and we have used the result on p. 367 of Dutton (1976). Without $\mathbf{K}$, this is the circulation theorem derived by Dutton (1976, p. 373).

Supercell models use the LES approach wherein the large energy-containing eddies are well resolved by the grid and the effects of the unresolved eddies are included via an eddy-viscosity parameterization for closure of the equations (Emanuel 1994, 290–297; MB16). Overbars and primes refer to resolved and unresolved parts of quantities, respectively. In tensor notation the frictional force is

$$F_i = \frac{1}{\rho}\frac{\partial\tau_{ij}}{\partial x_j}, \tag{15}$$

where

$$\tau_{ij} \equiv -\rho\overline{u_i' u_j'} \tag{16}$$

is the SGS stress tensor. Under the semislip condition, the shear stress in the surface layer is given by

$$\frac{\tau_{i3}}{\rho} = -C_D(|\mathbf{v}|u_i)|_{z=\Delta z/2}, \quad i=1,2, \tag{17}$$

where $C_D = [\kappa/\ln(\Delta z/2z_0)]^2$ is the drag coefficient, z_0 is the roughness length, and $\kappa \approx 0.4$ is von Kármán's constant (MB16). The free-slip condition is

$$\left.\frac{\tau_{i3}}{\rho}\right|_{z=0} = \left.\frac{\tau_{i3}}{\rho}\right|_{z=\Delta z}, \quad i=1,2. \tag{18}$$

For closure,

$$\frac{\tau_{ij}}{\rho} = K_m\left(\frac{\partial \overline{u}_i}{\partial x_j} + \frac{\partial \overline{u}_j}{\partial x_i}\right) - \frac{2}{3}\delta_{ij}\overline{e},$$
$$\overline{e} \equiv \frac{1}{2}\overline{u_i' u_i'}, \tag{19}$$

where K_m is the eddy viscosity and $\overline{e}$ is the turbulent kinetic energy (TKE). Similarly the turbulent theta-flux vector is

$$-\overline{u_i'\theta'} = K_h \frac{\partial \overline{\theta}}{\partial x_i}, \tag{20}$$

where K_h is the eddy diffusivity for heat. Following Deardorff (1972),

$$K_h = 3K_m. \tag{21}$$

To determine K_m, supercell models typically use a 1.5-order closure scheme involving the TKE (Emanuel 1994, 290–297). The eddy viscosity is related to TKE by

$$K_m = c_k \Delta \sqrt{\overline{e}}, \tag{22}$$

where c_k is a constant (typically 0.1) and Δ is an SGS length scale. Usually $\Delta = (\Delta x \Delta y \Delta z)^{1/3}$ where Δx, Δy, and Δz are the grid spacings in the x, y, and z directions.

A typical prognostic equation for TKE is

$$\frac{\partial \overline{e}}{\partial t} + \overline{u}_i \frac{\partial \overline{e}}{\partial x_i} = K_m \frac{\partial \overline{u}_i}{\partial x_j}\left(\frac{\partial \overline{u}_i}{\partial x_j} + \frac{\partial \overline{u}_j}{\partial x_i}\right) - 3K_m \frac{g}{\theta_0}\frac{\partial \overline{\theta}}{\partial z} + 2\frac{\partial}{\partial x_i}\left(K_m \frac{\partial \overline{e}}{\partial x_i}\right) - \frac{c_\varepsilon \overline{e}^{3/2}}{\Delta} \tag{23}$$

(Moeng and Wyngaard 1988, p. 3581), where the first and second terms on the right are the shear and buoyant generations of turbulence, the third term is turbulent diffusion of TKE, and the last term is the viscous dissipation $-\varepsilon$. The constant c_ε is typically 0.1. By definition, TKE cannot be negative so $\overline{e} \geq 0$ is enforced. With the appropriate initial and boundary conditions we can obtain the eddy viscosity K_m by solving (23) and (22). A trivial solution is $\overline{e} = 0$, so there may be regions where turbulence is absent. Under the free-slip condition (18), (23) indicates that a steady, horizontally uniform environment is nonturbulent at Richardson numbers

$$\mathrm{Ri} \equiv \frac{(g/\theta_0)(d\overline{\theta}/dz)}{(d\overline{u}/dz)^2} \geq \frac{1}{3}. \tag{24}$$

A weakness in the LES approach becomes apparent next to the ground. There the dynamically important eddies, which are very small near a solid boundary, are not resolved by the grid (Davidson 2015, p. 402). Furthermore, the mechanism of vorticity generation at the ground is not represented in LES. Physically, it is the *viscous* shear stress at the surface that generates vorticity, which then diffuses away from the boundary into the fluid (Davidson 2015, p. 51, 132, 403).

4. The Taylor–Proudman theorem

A steady, horizontally uniform environment without a heat source and Coriolis force is a solution of the governing equations for any wind profile $\mathbf{v}(z)$ if the lower boundary condition is free slip and the environment is turbulent free. On an f plane the situation is very different. The Taylor–Proudman theorem (Tritton 1988) only permits certain wind profiles. Adding an external force $\mathbf{K}(z)$ lifts the constraint by admitting superfluous solutions. We derive the theorem here since severe-storm modelers may not be familiar with it.

The Taylor–Proudman theorem is valid provided that the flow is quasi-steady, the Rossby number and Ekman number (ratio of frictional to Coriolis force) are much less than 1, the baroclinity vector $\mathbf{B}$ is small relative to the Coriolis parameter times the vertical wind shear (de la Torre Juárez 2009), and $\mathbf{K} \equiv 0$. Except close to the ground, all these conditions are met in the steady horizontally uniform environment of a supercell model prior to convective initiation.

From (1) the approximate equation of motion for a steady flow with small Ekman and Rossby numbers is

$$0 = -f\mathbf{k} \times \rho\mathbf{v} - \nabla p - g\rho\mathbf{k} + \mathbf{K}(z). \tag{25}$$

By taking the curl, and using vector identities, we obtain the relationship

$$0 = f\frac{\partial}{\partial z}(\rho\mathbf{v}) - f\mathbf{k}\,\cancel{\nabla \cdot (\rho\mathbf{v})} + g\mathbf{k} \times \nabla_H \rho + \nabla \times \mathbf{K}(z), \tag{26}$$

where ∇_H is the horizontal-gradient operator and the second term vanishes by mass conservation in (2) for steady flow. When $\mathbf{K}(z) \equiv 0$,

$$f\frac{\partial}{\partial z}(\rho\mathbf{v}) = 0 \tag{27}$$

above the PBL of a steady, horizontally uniform environment; that is, the momentum $\rho\mathbf{v}$ is independent of height. In a constant-density flow, $f\partial\mathbf{v}/\partial z = 0$. This is the Taylor–Proudman theorem, which states that in an incompressible or Boussinesq flow with $f \neq 0$ and $\mathbf{K}(z) \equiv 0$, the vertical shear must vanish for a steady solution to exist. This constraint explains the phenomenon of Taylor columns (Tritton 1988, p. 218). Note that (27) is just a slight generalization of the theorem. The Taylor–Proudman theorem is circumvented if either the environment is unsteady or extra degrees of freedom are manufactured.

5. Steady environment with winds that vary only with height

We now obtain solutions of the model equations that apply to a *static* ($\partial/\partial t = 0$) environment without a heat source ($\delta Q/\delta t = 0$) and with horizontally uniform winds $\mathbf{v}_0(z) = u_0(z)\mathbf{i} + v_0(z)\mathbf{j}$. The solutions are valid in a neighborhood of $(x, y) = (0, 0)$. We shall find once again that solutions exist only for specific conditions. Since environmental friction depends on the wind only, it is of the form $\mathbf{F}_0(z) \equiv G_0(z)\mathbf{i} + H_0(z)\mathbf{j}$. The invented force $\mathbf{K}(z) \equiv L_0(z)\mathbf{i} + M_0(z)\mathbf{j}$ by definition. Each thermodynamic field consists of a vertically varying base state, denoted by

subscript 0, and a deviation, which is smaller by at least an order of magnitude, with subscript 1. Thus,

$$\begin{aligned} p &= p_0(z) + p_1(x,y,z),\\ \rho &= \rho_0(z) + \rho_1(x,y,z), \qquad \text{and}\\ \theta &= \theta_0(z) + \theta_1(x,y,z). \end{aligned} \tag{28}$$

Inserting $\mathbf{v} = \mathbf{v}_0(z)$ and (28) into the governing equations in (1)–(4) yields

$$0 = -f\mathbf{k}\times\mathbf{v}_0(z) - \frac{1}{\rho_0(z)}\nabla_H p_1 + \mathbf{F}_0(z) + \mathbf{K}(z), \tag{29}$$

$$\partial p_0/\partial z = -g\rho_0, \quad \partial p_1/\partial z = -g\rho_1, \tag{30}$$

$$\mathbf{v}_0\cdot\nabla_H\rho_1 = 0, \tag{31}$$

$$\mathbf{v}_0\cdot\nabla_H\frac{\theta_1}{\theta_0} = \frac{D}{\theta_0}, \quad \text{and} \tag{32}$$

$$\frac{\theta_1}{\theta_0} = \frac{1}{\gamma}\frac{p_1}{p_0} - \frac{\rho_1}{\rho_0}. \tag{33}$$

In (29) the external force $\mathbf{K}$ is a surrogate for the HPGF so $\mathbf{K}\neq 0$ is used only when HPGF = 0 and vice versa. The steady-state continuity equation in (31) does not permit density advection when the environmental winds are horizontal uniform. The entropy equation in (32) represents a balance between advection and diffusion of entropy. When $\mathbf{K}\equiv 0$, the set (29)–(33) constitutes an overdetermined system of five equations in the three unknowns p_1, ρ_1, and θ_1. This system has solutions only in special circumstances.

In a neighborhood of $(x, y) = (0, 0)$, we may assume that the fields are linear in x and y. Thus, we let

$$p_1(x,y,z) = a(z)x + b(z)y, \tag{34}$$

where $a(z)\to 0$ and $b(z)\to 0$ as $z\to\infty$. Then from the hydrostatic equation in (30) and the equation of state equation in (33):

$$\rho_1(x,y,z) = -\frac{1}{g}\left[\frac{da(z)}{dz}x + \frac{db(z)}{dz}y\right] \quad \text{and} \tag{35}$$

$$\frac{\theta_1}{\theta_0} = \frac{1}{\gamma p_0}[a(z)x + b(z)y] + \frac{1}{g\rho_0}\left[\frac{da(z)}{dz}x + \frac{db(z)}{dz}y\right]. \tag{36}$$

Solutions for a steady hydrostatic environment exist only if the steady-state horizontal equations of motion, continuity equation, and the thermodynamic energy equation are satisfied. From (29), (31), (32), and (34)–(36), the conditions for a solution are

$$a = \rho_0(fv_0 + G_0 + L_0), \quad b = \rho_0(-fu_0 + H_0 + M_0), \tag{37}$$

$$-v_0\cdot\nabla_H\rho_1 = 0 = \frac{u_0}{g}\frac{da}{dz} + \frac{v_0}{g}\frac{db}{dz}, \quad \text{and} \tag{38}$$

$$\frac{1}{\gamma p_0}(u_0 a + v_0 b) + \frac{1}{gp_0}\left(u_0\frac{da}{dz} + v_0\frac{db}{dz}\right) = \frac{D_0}{\theta_0}. \tag{39}$$

In (39) we have set D to $D_0(z)$ because all other terms in (39) are functions of just height.

When $a = b = D_0 = 0$ and $\mathbf{K}\neq 0$, the system (37)–(39) always has a solution. This is the basis of the GWB method (section 8). We next consider the case in which p_1 is nonzero and $\mathbf{K}\equiv 0$. Even though $\mathbf{K}\equiv 0$, we retain it for completeness.

First there is the special case $\rho_1 = 0$ to examine. Then from (35) $da/dz = db/dz = 0$, which satisfies (38). Setting $da/dz = db/dz = 0$ in d/dz of (37) produces

$$f\mathbf{k}\times\frac{d(\rho_0\mathbf{v}_0)}{dz} = \frac{d[\rho_0(\mathbf{F}_0+\mathbf{K})]}{dz} \tag{40}$$

in vector form. According to (40), $d(\rho_0\mathbf{v}_0)/dz$ must vanish in the free atmosphere when $f\neq 0$ and $\mathbf{K}\equiv 0$. This is simply the generalized Taylor–Proudman theorem of section 4.

Next consider the more general case $\rho_1 > 0$. Inserting (37) into (38) yields

$$\begin{aligned} 0 = -\mathbf{v}_0\cdot\nabla_H\rho_1 &= -\frac{f}{g}\left[v_0\frac{d(\rho_0 u_0)}{dz} - u_0\frac{d(\rho_0 v_0)}{dz}\right]\\ &+ \frac{1}{g}\mathbf{v}_0\cdot\frac{d}{dz}[\rho_0(\mathbf{F}_0+\mathbf{K})] = -\frac{f\rho_0}{g}\left(v_0\frac{du_0}{dz} - u_0\frac{dv_0}{dz}\right)\\ &+ \frac{1}{g}\mathbf{v}_0\cdot\frac{d}{dz}[\rho_0(\mathbf{F}_0+\mathbf{K})]. \end{aligned} \tag{41}$$

The quantity $v_0 du_0/dz - u_0 dv_0/dz$ is the ground-relative helicity (GRH) density (Davies-Jones et al. 1990). Hence, only wind profiles without GRH density are allowed in the free atmosphere when $f\neq 0$ and $\mathbf{K}\equiv 0$. In contrast a tornado environment has a great deal of GRH above the PBL (Fig. 5) as demonstrated in the next section. Zero GRH density (shear vector parallel to ground-relative wind) occurs in an equivalent barotropic atmosphere, and is aptly referred to as inactive baroclinicity (Haltiner and Martin 1957, p. 409). Above the PBL, the isobars, isopycnics, and isentropes all must lie along the wind direction, which must be invariant with height because of $\mathbf{v}_0\cdot$(29) and (31)–(33). Otherwise, the solenoidal term generates vertical vorticity [see (12)] and hence horizontal gradients of the horizontal wind, which violates the assumption that $\mathbf{v} = \mathbf{v}_0(z)$.

We can also interpret our results from an energy perspective. From the scalar product of (29) with $\mathbf{v}_0$,

$$-\frac{1}{\rho_0}\mathbf{v}_0\cdot\nabla_H p_1 = -\mathbf{v}_0\cdot(\mathbf{F}_0+\mathbf{K}). \tag{42}$$

Friction dissipates kinetic energy so $\mathbf{v}_0\cdot\mathbf{F}_0 < 0$ [see the diagram in Haltiner and Martin (1957), p. 237]. Therefore positive work done by either the HPGF or the external force is the process that offsets frictional loss of kinetic energy in the environment. This means that for steady flow in the PBL the wind must have a component toward low pressure if there is an HPGF (Holton 1992, p. 133). From (42) and (31)–(33),

$$\mathbf{v}_0\cdot(\mathbf{F}_0+\mathbf{K}) = \frac{\gamma p_0}{\rho_0\theta_0}D_0, \tag{43}$$

which relates the work done by friction and the external force to turbulent diffusion of thermal energy. Above the PBL

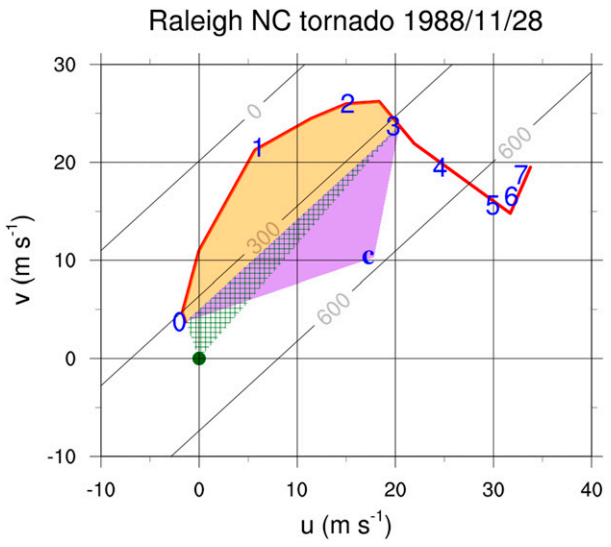

FIG. 5. Environmental ground-relative hodograph for the Raleigh, North Carolina, violent tornado on 28 Nov 1988. The green dot marks the origin. Blue numbers along the red hodograph curve denote height AGL (km). The blue **c** indicates the observed storm motion vector (240° at 20.6 m s^{-1}). All areas are algebraic ones. These are *negative* when they are swept out by a wind vector that turns *clockwise* with height. Helicities are minus 2 times the corresponding area. The orange area bounded by the hodograph curve and the 0–3-km shear vector is $-165\,\mathrm{m^2\,s^{-2}}$. The area of the solid purple triangle defined by the shear vector and the tip of **c** is $-120\,\mathrm{m^2\,s^{-2}}$. Thus, the SRH for the lowest 3 km is $-2(-165-120) = 570\,\mathrm{m^2\,s^{-2}}$. The orange area arises from the hodograph turning clockwise with height, and the purple area arises from storm motion to the right of the shear vector. Likewise, the 0–3-km GRH is minus 2 times the sum of the orange area and the green-hatched triangular area or $439\,\mathrm{m^2\,s^{-2}}$. Equally spaced straight lines parallel to the 0–3-km shear vector are 0, 300, and $600\,\mathrm{m^2\,s^{-2}}$ contours of helicity as a function of **c**. For the 0–1-km layer, the SRH is $330\,\mathrm{m^2\,s^{-2}}$ and the GRH is $91\,\mathrm{m^2\,s^{-2}}$. [This figure is similar to the figure in Davies-Jones et al. (1990) but is for the unmodified 0000 UTC Greensboro, North Carolina, sounding].

thermal diffusion has to balance any work performed by the external force.

Since supercell models conserve mass only approximately (section 3), a good question is what happens when the pseudoincompressible continuity equation in (10) is used instead of (31). In this situation, the density advection, $-\mathbf{v}_0\cdot\nabla_H\rho_1$, is no longer constrained to be zero. By substituting for the advection terms via (42) and (41) (without the leading "0 = "), we find that the entropy equation in (32) after use of (33) provides the following condition for a solution:

$$\frac{\rho_0}{\gamma p_0}\mathbf{v}_0\cdot(\mathbf{F}_0+\mathbf{K})+\frac{1}{g\rho_0}\mathbf{v}_0\cdot\frac{d}{dz}[\rho_0(\mathbf{F}_0+\mathbf{K})] -\frac{f}{g}\left(v_0\frac{du_0}{dz}-u_0\frac{dv_0}{dz}\right)=\frac{D_0}{\theta_0}. \tag{44}$$

Even with the weak form of mass conservation, solutions with $\mathbf{K}\equiv 0$ exist in the free atmosphere only when the GRH density is zero there.

6. Tornadic-storm environments

We now demonstrate that the condition for a steady solution without an invented force of the governing equations for the environment, zero GRH density above the PBL, is uncharacteristic of tornado proximity soundings. The equations of motion for hydrostatic flow on an f plane at small Rossby number are

$$\begin{aligned} 0&=fv-\alpha\partial p/\partial x+(\mathbf{F}+\mathbf{K})\cdot\mathbf{i},\\ 0&=-fu-\alpha\partial p/\partial y+(\mathbf{F}+\mathbf{K})\cdot\mathbf{j}, \qquad \text{and}\\ g\rho&=-\partial p/\partial z. \end{aligned} \tag{45}$$

From (45) it follows that the GRH density is

$$\mathbf{v}\cdot\boldsymbol{\omega}\equiv v\frac{\partial u}{\partial z}-u\frac{\partial v}{\partial z}=\frac{\mathbf{v}}{f}\cdot\left[g\nabla_H\ln\rho-\frac{\partial\alpha}{\partial z}\nabla_H p+\frac{\partial}{\partial z}(\mathbf{F}+\mathbf{K})\right], \tag{46}$$

where $\boldsymbol{\omega}=-\mathbf{i}\partial v/\partial z+\mathbf{j}\partial u/\partial z$ is the relative-vorticity vector. Through suitable choice of the invented force $\mathbf{K}(z)$, we can obtain a horizontally uniform environment that has the same GRH density as an observed hodograph. Via conversion to pressure coordinates, the hydrostatic equation and the equation of state ($p=\rho RT$), we obtain the following relationship:

$$g\nabla_H\ln\rho-\frac{\partial\alpha}{\partial z}\nabla_H p=g\nabla_p\ln\rho=-g\nabla_p\ln T, \tag{47}$$

where ∇_p is the operator $\mathbf{i}(\partial/\partial x)_p+\mathbf{j}(\partial/\partial y)_p$. Then (46) becomes

$$\mathbf{v}\cdot\boldsymbol{\omega}=-\frac{g}{fT}\mathbf{v}\cdot\nabla_p T+\frac{1}{f}\mathbf{v}\cdot\frac{\partial\mathbf{F}}{\partial z}+\frac{1}{f}\mathbf{v}\cdot\frac{\partial\mathbf{K}}{\partial z}. \tag{48}$$

Thus, GRH density always depends on the scalar product of the wind with the vertical derivative of the frictional force. It also depends on warm-air advection on isobaric surfaces if the environment is unconstrained, or on the vertical derivative of the invented force if the environment is compelled to be horizontally uniform.

The ground-relative helicity is defined by

$$\mathrm{GRH}\equiv\int_{h_1}^{h_2}\mathbf{v}(z)\cdot\boldsymbol{\omega}(z)\,dz, \tag{49}$$

where h_1 and h_2 nominally define the effective base and top of the storm's inflow layer (typically $h_1=0$ and $h_2=3$ or 1 km). The GRH is minus 2 times the area swept out from $z=h_1$ to h_2 by the ground-relative wind vector $\mathbf{v}(z)$ (Fig. 5; Davies-Jones et al. 1990). Note that the area swept out by the geostrophic wind is proportional to geostrophic warm-air advection (Haltiner and Martin 1957, p. 209). GRH is additive. In other words, the GRH for the 0–h_2 layer is equal to the sum of the 0–h_1 and h_1–h_2 GRHs. From (48) and (49), the GRH is

$$\mathrm{GRH}=\int_{h_1}^{h_2}\left(-\frac{g}{fT}\mathbf{v}\cdot\nabla_p T\right)dz+\int_{h_1}^{h_2}\left[\frac{1}{f}\mathbf{v}\cdot\frac{\partial(\mathbf{F}+\mathbf{K})}{\partial z}\right]dz. \tag{50}$$

The terms on the right are due to thermal advection, friction, and the artificial force. Warm advection of 1 K h^{-1} contributes approximately $100\,\mathrm{m^2\,s^{-2}}$ of GRH per 1 km of inflow depth.

We find the GRH associated with an Ekman layer by neglecting thermal advection and **K**, assuming constant eddy viscosity so that $\mathbf{F} = K_m(\mathbf{i}d^2u/dz^2 + \mathbf{j}d^2v/dz^2)$, and plugging in the standard Ekman-layer solution (Holton 1992, 129–130). The result is

$$\text{GRH} = \int_0^\infty \mathbf{v}\cdot\boldsymbol{\omega}\,dz = \int_0^\infty \frac{1}{f\rho}\mathbf{v}\cdot\frac{\partial}{\partial z}(\rho\mathbf{F})\,dz = \frac{1}{2}|\mathbf{v}_g|^2 \qquad (51)$$

(Davies-Jones et al. 1990), where $\mathbf{v}_g$ is the geostrophic wind. For $|\mathbf{v}_g| = 14\,\text{m s}^{-1}$, the GRH of the Ekman layer is $100\,\text{m}^2\,\text{s}^{-2}$.

The storm-relative helicity (SRH) is similar to the GRH except the relevant wind is the storm-relative one, $\mathbf{v} - \mathbf{c}$, where **c** is the storm motion vector. It is a measure of how favorable the environmental wind profile is for tornado development (Davies-Jones et al. 1990; Droegemeier et al. 1993). SRH is defined by

$$\text{SRH} \equiv \int_{h_1}^{h_2} [\mathbf{v}(z) - \mathbf{c}]\cdot\boldsymbol{\omega}\,dz. \qquad (52)$$

The SRH is minus 2 times the area swept out from $z = h_1$ to h_2 by the storm-relative wind vector (Fig. 5; Davies-Jones et al. 1990). The integrand in (52) is the SRH density. It is an important quantity because it is linked theoretically to overall updraft rotation. In an updraft with a quasi-circular cross section, the covariance of vertical velocity and vertical vorticity is proportional to it (Davies-Jones 1984). From (52) and (51), the SRH is

$$\text{SRH} = \text{GRH} + \mathbf{k}\cdot\mathbf{c}\times[\mathbf{v}_0(h_2) - \mathbf{v}_0(h_1)], \qquad (53)$$

where $\mathbf{v}_0(h_2) - \mathbf{v}_0(h_1)$ is the h_1–h_2 shear vector. The last term in (53) is the part of SRH due to storm motion to the right of this shear vector and the integral is the GRH. Like GRH, SRH is additive.

Figure 5 shows an example of a proximity hodograph for a violent tornado that occurred in the warm sector of a cyclone. In this case, the GRH for the 0–1-km layer is $91\,\text{m}^2\,\text{s}^{-2}$ over the nominal height of the PBL (0–1 km) and is much higher, $439\,\text{m}^2\,\text{s}^{-2}$, for the 0–3-km layer. The 0–1- and 0–3-km SRH values, 330 and $570\,\text{m}^2\,\text{s}^{-2}$, respectively, are even higher because of storm motion to the right of the corresponding shear vectors. In this case as well as in the mean tornado-outbreak proximity hodograph [see Fig. 11 of Maddox (1976)], large GRH and veering wind direction above the PBL indicate that an atmosphere favorable for tornadoes is far from equivalent barotropic.

There is not a large 0–1-km GRH in Fig. 5 because there is not much near-ground warm-air advection in a warm sector. For storms just ahead of warm fronts, there is large environmental GRH near the surface from strong warm advection (Maddox et al. 1980). The geostrophic warm-air advection contribution to GRH is also associated with synoptic-scale upward motion and airmass destabilization (Holton 1992). A significant invented force is necessary to compensate for lack of thermal advection if the environment is forced to be horizontally uniform.

Equation (50) for GRH has only thermal advection and friction terms because we have assumed small Rossby number. Many tornado outbreaks are associated with small-scale ageostrophic circulations that change rapidly on a time scale of a few hours. Our assumption of small Rossby number is invalid at these scales. Such ageostrophic circulations may form in association with shortwave troughs, jet streaks, low-level jets, boundaries, mesolows, dryline bulges, upslope winds, and diurnal wind oscillations (Maddox 1993). They can set the stage for tornado development by swiftly increasing low-level wind veering and helicity. Thus, significant amounts of GRH in a hodograph may arise from ageostrophic winds. Modeling these situations really requires a mesoscale model.

7. The frictional balancing procedure

The frictional balancing procedure assumes falsely that the winds in the actual hodograph are geostrophic at all heights. It also neglects the horizontal temperature gradient associated with thermal-wind balance. The negative of the Coriolis force acting on the environmental geostrophic wind is the external force in this method (Fig. 2). Adding this force is equivalent to letting the Coriolis force act only on deviations from the environmental geostrophic wind. The model is then run without a storm until it reaches a steady state. The ageostrophic part of the Coriolis force is now in balance with the frictional force (Fig. 2). The ageostrophic wind so determined is added to the "geostrophic hodograph" to form an "input hodograph," which is steady because there is a three-way force balance in its PBL between the external, the Coriolis, and the parameterized frictional forces.

When $p_1 = a = b = 0$ the system in (37)–(39) has the following solution:

$$G_0 + L_0 = -fv_0,\quad H_0 + M_0 = fu_0,\quad \text{and}\quad D_0 = 0. \qquad (54)$$

In the FBP the three-force balance is assumed arbitrarily to consist of the following two two-force balances (Fig. 2):

$$\mathbf{K}(z) \equiv L_0\mathbf{i} + M_0\mathbf{j} = -fv_g\mathbf{i} + fu_g\mathbf{j} \qquad \text{and}$$
$$\mathbf{F}_0(z) \equiv G_0\mathbf{i} + H_0\mathbf{j} = -fv_{ag}\mathbf{i} + fu_{ag}\mathbf{j}, \qquad (55)$$

where $\mathbf{v}_g$ are the winds in the geostrophic hodograph and $\mathbf{v}_{ag}$ are the additional winds needed to form the input hodograph $\mathbf{v}_0(z)$ from the geostrophic one. In FBP, the external force **K** cancels the geostrophic part of the Coriolis force. The FBP hodograph modification reduces the ground-relative surface wind and creates a significant ageostrophic wind. These changes enable the Coriolis force acting on the ageostrophic wind to balance the frictional force at the ground as required by (55). We can deduce the frictional force from the difference in the two hodographs in Fig. 1 of R20.

However, separating wind into geostrophic and ageostrophic parts from a single sounding is impossible, and (55) merely increases the number of variables without adding any meaningful information. Adding the equations in (55) together yields

$$0 = -f\mathbf{k}\times\mathbf{v}_0(z) + \mathbf{K}(z) + \mathbf{F}_0(z), \qquad (56)$$

which recovers the three-force balance in the PBL of the input environment. We can obtain **K** from (56) using GWB (section 8),

and (unnecessarily) determine $\mathbf{v}_g$ from the ambiguous (55). As long as the same hodograph is input to the model, as is the case with the R16 and RX17 FBP simulations, and the R20 GWB simulations, GWB subsumes FBP and renders it redundant.

8. The geotriptic wind balance method

The geotriptic wind balance method (GWB) purportedly uses a horizontally uniform environment that is hydrostatically balanced and in three-way equilibrium between the Coriolis force, the parameterized turbulent frictional force, and the HPGF. Unfortunately, such equilibrium is strictly impossible in a *sheared horizontally uniform* environment with a Coriolis force because, above the PBL, the wind shear is in thermal-wind balance with the large-scale *horizontal temperature gradient*, which has been set to zero. In a hydrostatic environment, the hydrostatic equation and the ideal gas law link the pressure and virtual temperature fields to the horizontal momentum equation. To preserve a horizontally uniform steady environment, "the large-scale PGF must somehow be specified and *decoupled* from the actual model pressure field" (DRX19, p. 3936). To accomplish this, an external force again is used that enables the environmental HPGF to vanish. The external force in GWB is the negative of the resultant of the Coriolis force acting on the environmental wind and the environmental friction (Fig. 3). By adding the external force permanently to the horizontal equation of motion, the environment is maintained throughout the simulation.

GWB controls the environment with the horizontal invented force in (56):

$$\mathbf{K}(z) \equiv L_0(z)\mathbf{i} + M_0(z)\mathbf{j} = (-fv_0 - G_0)\mathbf{i} + (fu_0 - H_0)\mathbf{j}. \quad (57)$$

In GWB $\mathbf{K}$ is called the pseudo–pressure-gradient force (PPGF) because it replaces the HPGF in the three-force balance (Fig. 3). Introducing this force provides two more degrees of freedom L_0 and M_0 and, thus, allows solutions for all wind profiles. It neglects the horizontal temperature gradient associated with thermal-wind balance (R20, p. 3375). In the environment there is only geostrophic wind balance in the free atmosphere and the three-force balance within the PBL. It is easily verified that (57) and $p_1 = \rho_1 = D_0 = 0$ satisfy (29)–(32), which govern the steady environment.

To obtain a 3D steady, horizontally uniform environment, DRX19 (p. 3938) and R20 ran the model without initiating a storm and without the external force. Since $\mathbf{K}(z)$ is the force needed to equilibrate the Coriolis and frictional forces, it is then determined as minus the horizontal average of the initial tendency of $\mathbf{v}_H$. Including $\mathbf{K}(z)$ establishes a steady-state solution for any environmental wind profile. Since (32) implies $D_0 = 0$ in steady, horizontally uniform flow, the resulting PBL is well mixed. Figure 1 shows the balance of forces in the environment above the PBL. Because $\mathbf{K}$ counterbalances both the environmental frictional force and the Coriolis force acting on the environmental wind, f is in effect zero for flow in the undisturbed steady environment. The Taylor–Proudman theorem (section 4), which only applies to flows with small Rossby and Ekman numbers, is undone because the Rossby number for the environment is now effectively infinite instead of much less than one. Inclusion of the external force has eliminated the nagging Taylor–Proudman theorem (and the thermal wind and Taylor columns for good measure). The replacement of the HPGF by the PPGF $\mathbf{K}$ has a dramatic effect. It decouples the horizontal equation of motion from the hydrostatic equation, thus, allowing the much coveted, steady, horizontally uniform environment to be attained. There are no longer horizontal gradients or advection of any thermodynamic variable in the environment. The significant GRH density above the PBL that exists in tornado environments (section 6) is kept in the model artificially through the force substitution. From the energy perspective, (42) indicates that in GWB the spurious work rate $\mathbf{v}_0 \cdot \mathbf{K}$ has to offset the frictional loss of environmental kinetic energy $-\mathbf{v}_0 \cdot \mathbf{F}_0$. Work performed by the environmental HPGF would supply this energy in real tornado environments.

In GWB the environmental wind profile is immutable by the decree that declares the environmental forces are always in equilibrium. This is true even when resolved turbulence is present because its effects on the wind profile are nullified by then varying the PPGF at every time step to maintain the equilibrium (DRX19, p. 3945). (In this case the made-up force is a function of t as well as z.)

A solution of (23) is TKE = 0, which signifies that the SGS turbulence scheme is inactive. This can happen in the environment of simulations with the free-slip lower boundary condition. Since there are no eddies (MB16, p. 1848), resolution of important eddies near the ground is not an issue. To obtain a deep turbulent boundary layer in neutral stratification with surface drag, MB16 introduced random temperature perturbations of significant amplitude (0.25 K) to promote vertical mixing. With surface drag and without excitation of significant turbulence, there is a danger in GWB that the environment's neutral boundary layer is too shallow and that the shear in the lowest few hundred meters is too large (MB16).

Additional problems arise because GWB adds the significant permanent artificial force $\mathbf{K}(z)$ and its associated torque $d\mathbf{K}/dz$ everywhere. Within the storm, the frictional and Coriolis forces do not counterbalance the permanent and pervasive PPGF. Eliminating $\mathbf{K}$ from (1) via (57) exposes the deleterious effect of this procedure. We obtain

$$\frac{d\mathbf{v}}{dt} = -f\mathbf{k} \times [\mathbf{v} - \mathbf{v}_0(z)] - \frac{1}{\rho}\nabla p - g\mathbf{k} + [\mathbf{F} - \mathbf{F}_0(z)]. \quad (58)$$

Instead of just the local friction we have an effective frictional force, which is the difference between the local friction and friction at the same height in the environment. Similarly, the Coriolis force acts not on the wind itself but on the deviation of the wind from the environmental wind on the same level. From a diagram of the three-force balance (Fig. 3) within the environmental PBL, it is evident that an unbalanced fake force acts to accelerate parcels downwind and to the left of the environmental wind at the same height. Because the artificial force varies markedly with height next to the ground (Fig. 8 in DRX19), it produces excessive shear there. Markowski (2016) also added a term to the horizontal equations of motion to minimize the evolution of the environment, but the size of his term was small enough to have minor effect on the vorticity and circulation budgets.

Permanence of **K** also affects the circulation analyses. R20's simulations with a nonzero drag coefficient produce early tornadoes. The surface drag causes circulation gain around a material circuit by retarding near-surface parcels whose velocity is contributing negatively to the circulation while having little effect on higher parcels in the circuit. To examine the effect of GWB on this result, we substitute (57) into (14) to eliminate **K**. This yields the following circulation theorem for GWB:

$$\frac{d}{dt}\oint_{C(t)} \mathbf{v}\cdot d\mathbf{x} = \oint_{C(t)} p\, d\alpha - f\oint_{C(t)} \mathbf{k}\times[\mathbf{v}-\mathbf{v}_0(z)]\cdot d\mathbf{x} + \oint_{C(t)} [\mathbf{F}-\mathbf{F}_0(z)]\cdot d\mathbf{x}. \tag{59}$$

Since the environment is horizontally uniform in GWB, there are no solenoids there. Thus, in the steady horizontally uniform environment, all the terms in (59) vanish. The **K** term in (14) has been dismissed as an ''artifact.'' However, the last term in (59) reveals that the main consequence of **K** is to effectively change the frictional-force circulation to the line integral of $\mathbf{F}-\mathbf{F}_0(z)$ instead of just **F**. Considering only the line integral of **F** can lead to false conclusions about the role of surface drag in tornadogenesis. Because the bogus force **K** also alters the path and configuration of the material circuit $C(t)$, results of the circulation analyses seem doubtful.

Hence the spurious circulation [the last term in (14)] cannot be dismissed. Figure 11 of R20 shows the (positive) circulation around a material circuit and the production terms as functions of drag coefficient from time $t = 23$ min, when the circuit is a horizontal low-level circle of radius 1.5 km encircling the developing tornado back to $t = 13$ min. Since **K** is a function just of z, the artificial term vanishes when a circuit is flat. This behavior is evident in the R20 Fig. 11. At the end of the backward trajectories at 13 min., the spurious production term is positive in all the experiments and it is the largest in all but one. By reasonable extrapolation of the curves to the initial time $t = 0$, it seems probable that the artificial term produces most of the circulation in the simulations with no to moderate surface drag.

9. Conclusions

Without an externally imposed force, a steady environment with horizontally uniform winds is possible only if the winds in the free atmosphere are parallel to the isobars, isotherms, and isopycnics. Because a horizontal temperature gradient is accompanied by vertical shear and entropy is conserved, these conditions only hold for winds that are unidirectional above the friction layer and consequently for environments with little ground-relative helicity. With vertical wind shear and Coriolis force, a steady, horizontal uniform solution is possible for any wind profile *only if* the horizontal equation of motion becomes decoupled from the hydrostatic equation. This is achieved through the use of an artificial force, which enables the Taylor–Proudman theorem to be circumvented.

Maintaining an ideal, steady, horizontally uniform, sheared environment in a supercell model with Coriolis and frictional forces comes at a cost to the dynamics. The most recent method introduces a permanent omnipresent made-up horizontal force $\mathbf{K}(z)$ that accelerates all parcels all the time. It balances the model's Coriolis and horizontal frictional forces prior to convective initiation. It performs illusory work that in the prestorm environment offsets kinetic energy dissipated by friction. It unnaturally uncouples the environmental horizontal equation of motion from the hydrostatic equation and severs the dynamics from the thermodynamics. Addition of the extraneous force has the same effect as changing the local frictional force from **F** to $\mathbf{F}-\mathbf{F}_0(z)$, where $\mathbf{F}_0(z)$ is the frictional force at the same height z in the environment, and similarly altering the Coriolis force.

Moreover $\nabla\times\mathbf{K}(z)$ fabricates excessive horizontal vorticity very close to the ground so there is also a substantial spurious circulation. **K** also changes the parcel trajectories, which further affects the material vorticity and circulation analyses.

In recent simulations with surface drag and powerful initiation, tornadoes develop from frictionally generated vorticity atypically early in the lifetime of their parent supercells and far from precipitation. Although vortices such as waterspouts and landspouts occur early in the life cycles of their parent clouds, they form in environments that are not horizontally homogeneous. Occasionally tornadoes form in young supercell storms, but little is known about their mesoscale environments and their causes. Revealingly, low-precipitation supercells produce relatively few tornadoes (Davies-Jones et al. 1976; Bluestein and Parks 1983). If supercell tornadoes form just from low-level cloud-scale convergence and rotation plus surface drag, they would occur much more frequently and generally much earlier in the life cycle of the parent supercell.

Rapid tornadogenesis in simulations may be due to a combination of the following factors:

1) excessively strong convective initiation in a very unstable atmosphere, resulting in too strong a low-level updraft too early in a supercell's lifetime,
2) use of the semislip lower boundary condition,
3) absence of perturbations to excite significant turbulence, resulting in too strong a frictional force and too much shear in too shallow a layer next to the ground (MB16), and
4) use of an omnipresent, pervasive external force to maintain a steady, horizontally uniform environment; this force introduces extra degrees of freedom that allow the Taylor–Proudman theorem to be circumvented but has the unintended consequence of altering the dynamics inside the storm.

A possible mechanism for rapid tornadogenesis in a simulation is as follows. As a result of factor 4, the external force is fixed by the three-force balance in the environment. It is concentrated near the ground by factors 2 and 3. Inside the storm, friction and the Coriolis force no longer balance it so it generates large amounts of horizontal vorticity in a shallow surface-based layer. Tilting and stretching of this vorticity (if it happens to be streamwise) by the updraft in factor 1 will produce significant vertical vorticity at low heights (as demonstrated by Rotunno et al. 2017).

The advices for supercell modelers are threefold. First, do not initiate convection violently and expect early storm development

to be realistic. Second, introduce random perturbations of sufficient strength to obtain a deep turbulent PBL. Third, do not resort to an artificial force that decouples the horizontal momentum and hydrostatic equations and generates spurious energy and vorticity.

Acknowledgments. Valuable comments by Drs. Paul Markowski and Louis Wicker and the three anonymous reviewers prompted significant improvements in the paper.

REFERENCES

Adlerman, E. J., and K. K. Droegemeier, 2002: The sensitivity of numerically simulated cyclic mesocyclogenesis to variations in model physical and computational parameters. *Mon. Wea. Rev.*, **130**, 2671–2691, https://doi.org/10.1175/1520-0493(2002)130<2671:TSONSC>2.0.CO;2.

Bluestein, H. B., and C. R. Parks, 1983: A synoptic and photographic climatology of low-precipitation severe thunderstorms in the southern plains. *Mon. Wea. Rev.*, **111**, 2034–2046, https://doi.org/10.1175/1520-0493(1983)111<2034:ASAPCO>2.0.CO;2.

Coffer, B. E., and M. D. Parker, 2017: Simulated supercells in nontornadic and tornadic VORTEX2 environments. *Mon. Wea. Rev.*, **145**, 149–180, https://doi.org/10.1175/MWR-D-16-0226.1.

Dahl, J. M. L., M. D. Parker, and L. J. Wicker, 2012: Uncertainties in trajectory calculations within near-surface mesocyclones of simulated supercells. *Mon. Wea. Rev.*, **140**, 2959–2966, https://doi.org/10.1175/MWR-D-12-00131.1.

Davidson, P. A., 2015: *Turbulence: An Introduction for Scientists and Engineers.* 2nd ed. Oxford University Press, 630 pp.

Davies-Jones, R. P., 1984: Streamwise vorticity: The origin of updraft rotation in supercell storms. *J. Atmos. Sci.*, **41**, 2991–3006, https://doi.org/10.1175/1520-0469(1984)041<2991:SVTOOU>2.0.CO;2.

——, 2002: Linear and nonlinear propagation of supercell storms. *J. Atmos. Sci.*, **59**, 3178–3205, https://doi.org/10.1175/1520-0469(2003)059<3178:LANPOS>2.0.CO;2.

——, D. W. Burgess, and L. R. Lemon, 1976: An atypical tornado-producing cumulonimbus. *Weather*, **31**, 337–347, https://doi.org/10.1002/j.1477-8696.1976.tb07449.x.

——, ——, and M. Foster, 1990: Test of helicity as a forecast parameter. Preprints, *16th Conf. on Severe Local Storms*, Kananaskis Park, AB, Canada, Amer. Meteor. Soc., 588–592.

Dawson, D. T., B. Roberts, and M. Xue, 2019: A method to control the environmental wind profile in idealized simulations of deep convection with surface friction. *Mon. Wea. Rev.*, **147**, 3935–3954, https://doi.org/10.1175/MWR-D-18-0462.1.

de la Torre Juárez, M., 2009: Taylor–Proudman columns in non-hydrostatic divergent baroclinic and barotropic flows. *Quart. J. Roy. Meteor. Soc.*, **135**, 2179–2184, https://doi.org/10.1002/qj.483.

Deardorff, J. W., 1972: Numerical investigation of neutral and unstable planetary boundary layers. *J. Atmos. Sci.*, **29**, 91–115, https://doi.org/10.1175/1520-0469(1972)029<0091:NIONAU>2.0.CO;2.

Droegemeier, K. K., S. M. Lazarus, and R. Davies-Jones, 1993: The influence of helicity on numerically simulated convective storms. *Mon. Wea. Rev.*, **121**, 2005–2029, https://doi.org/10.1175/1520-0493(1993)121<2005:TIOHON>2.0.CO;2.

Durran, D. R., 1989: Improving the anelastic approximation. *J. Atmos. Sci.*, **46**, 1453–1461, https://doi.org/10.1175/1520-0469(1989)046<1453:ITAA>2.0.CO;2.

Dutton, J. A., 1976: *The Ceaseless Wind.* McGraw-Hill, 579 pp.

Emanuel, K. A., 1994: *Atmospheric Convection.* Oxford University Press, 580 pp.

Fiedler, B., and R. Rotunno, 1986: A theory for the maximum wind speeds in tornado-like vortices. *J. Atmos. Sci.*, **43**, 2328–2340, https://doi.org/10.1175/1520-0469(1986)043<2328:ATOTMW>2.0.CO;2.

Haltiner, G. J., and F. L. Martin, 1957: *Dynamical and Physical Meteorology.* McGraw-Hill, 470 pp.

Holton, J. R., 1992: *An Introduction to Dynamic Meteorology*, 3rd ed. Academic Press, 511 pp.

Klemp, J. B., and R. B. Wilhelmson, 1978: The simulation of three-dimensional convective storm dynamics. *J. Atmos. Sci.*, **35**, 1070–1096, https://doi.org/10.1175/1520-0469(1978)035<1070:TSOTDC>2.0.CO;2.

Maddox, R. A., 1976: An evaluation of tornado proximity wind and stability data. *Mon. Wea. Rev.*, **104**, 133–142, https://doi.org/10.1175/1520-0493(1976)104<0133:AEOTPW>2.0.CO;2.

——, 1993: Diurnal low-level wind oscillation and storm-relative helicity. *The Tornado: Its Structure, Dynamics, Prediction, and Hazards*, *Geophys. Monogr.*, Vol. 79, Amer. Geophys. Union, 591–598.

——, L. F. Hoxit, and C. F. Chappel, 1980: A study of tornadic thunderstorm interactions with thermal boundaries. *Mon. Wea. Rev.*, **108**, 322–336, https://doi.org/10.1175/1520-0493(1980)108<0322:ASOTTI>2.0.CO;2.

Markowski, P. M., 2016: An idealized numerical simulation investigation of the effects of surface drag on the development of near-surface vertical vorticity in supercell thunderstorms. *J. Atmos. Sci.*, **73**, 4349–4385, https://doi.org/10.1175/JAS-D-16-0150.1.

——, and G. Bryan, 2016: LES of laminar flow in the PBL: A potential problem for convective storm simulations. *Mon. Wea. Rev.*, **144**, 1841–1850, https://doi.org/10.1175/MWR-D-15-0439.1.

Mashiko, W., 2016: A numerical study of the 6 May 2012 Tsukuba City supercell tornado. Part I: Vorticity sources of low-level and midlevel mesocyclones. *Mon. Wea. Rev.*, **144**, 1069–1092, https://doi.org/10.1175/MWR-D-15-0123.1.

Moeng, C.-H., and J. C. Wyngaard, 1988: Spectral analysis of large-eddy simulations of the convective boundary layer. *J. Atmos. Sci.*, **45**, 3573–3587, https://doi.org/10.1175/1520-0469(1988)045<3573:SAOLES>2.0.CO;2.

Oliveira, M. I., M. Xue, B. J. Roberts, L. J. Wicker, and N. Yussouf, 2019: Horizontal vortex tubes near a simulated tornado: Three-dimensional structure and kinematics. *Atmosphere*, **10**, 716, https://doi.org/10.3390/atmos10110716.

Roberts, B., and M. Xue, 2017: The role of surface drag in mesocyclone intensification leading to tornadogenesis within an idealized supercell simulation. *J. Atmos. Sci.*, **74**, 3055–3077, https://doi.org/10.1175/JAS-D-16-0364.1.

——, ——, A. D. Schenkman, and D. T. Dawson, 2016: The role of surface drag in tornadogenesis within an idealized supercell simulation. *J. Atmos. Sci.*, **73**, 3371–3405, https://doi.org/10.1175/JAS-D-15-0332.1.

——, ——, and D. T. Dawson, 2020: The effect of surface drag strength on mesocyclone intensification and tornadogenesis in idealized supercell simulations. *J. Atmos. Sci.*, **77**, 1699–1721, https://doi.org/10.1175/JAS-D-19-0109.1.

Rotunno, R., P. M. Markowski, and G. H. Bryan, 2017: "Near ground" vertical vorticity in supercell thunderstorm models.

J. Atmos. Sci., **74**, 1757–1766, https://doi.org/10.1175/JAS-D-16-0288.1.

Schenkman, A. D., M. Xue, and M. Hu, 2014: Tornadogenesis in a high-resolution simulation of the 8 May 2003 Oklahoma City supercell. *J. Atmos. Sci.*, **71**, 130–154, https://doi.org/10.1175/JAS-D-13-073.1.

Tao, T., and T. Tamura, 2020: Numerical study of the 6 May 2012 Tsukuba supercell tornado: Vorticity sources responsible for tornadogenesis. *Mon. Wea. Rev.*, **148**, 1205–1228, https://doi.org/10.1175/MWR-D-19-0095.1.

Tritton, D. J., 1988: *Physical Fluid Dynamics.* 2nd ed. Clarendon, 519 pp.

Wilhelmson, R. B., and C.-S. Chen, 1982: A simulation of the development of successive cells along a cold outflow boundary. *J. Atmos. Sci.*, **39**, 1466–1483, https://doi.org/10.1175/1520-0469(1982)039<1466:ASOTDO>2.0.CO;2.

——, and L. J. Wicker, 2001: Numerical modeling of severe local storms. *Severe Convective Storms, Meteor. Monogr.*, No. 50, Amer. Meteor. Soc., 123–166.